

The Food Matrix and the Gastrointestinal Fluids Alter the Features of Silver Nanoparticles

Laurie Laloux, Donika Kastrati, Sébastien Cambier, Arno C. Gutleb,*
and Yves-Jacques Schneider*

Silver nanoparticles (AgNPs) are used in the agri-food sector, which can lead to their ingestion. Their interaction with food and their passage through the gastrointestinal tract can alter their properties and influence their fate upon ingestion. Therefore, this study aims at developing an *in vitro* method to follow the fate of AgNPs in the gastrointestinal tract. After incorporation of AgNPs into a standardized food matrix, a precolonic digestion is simulated and AgNPs are characterized by different techniques. The presence of food influences the AgNPs properties by forming a corona around nanoparticles. Even if the salivary step does not impact significantly the AgNPs, the pH decrease and the digestive enzymes induce the agglomeration of AgNPs during the gastric phase, while the addition of intestinal fluids disintegrates these clusters. AgNPs can thus reach the intestinal cells under nanometric form, although the presence of food and gastrointestinal fluids modifies their properties compared to pristine AgNPs. They can form a corona around the nanoparticles and act as colloidal stabilizer, which can impact the interaction of AgNPs with intestinal epithelium. This study demonstrates the importance of taking the fate of AgNPs in the gastrointestinal tract into account to perform an accurate risk assessment of nanomaterials.

their unique properties and therefore they are used for various purposes from farm-to-fork. For instance, in agriculture, AgNPs might be helpful to hinder plant diseases caused by fungi^[6] and they are also employed in animal husbandry as a disinfectant.^[7] In the food sector, AgNPs are incorporated in food containers or into fridges to inhibit microbial development. They are also employed in food packaging and incorporated in kitchenware and tableware as an antimicrobial coating.^[8] AgNPs are thus generally not added directly to food.^[9] However, migration of AgNPs and silver ions (Ag⁺) from packaging and containers has been shown in various studies.^[10–12] Besides that, they have recently been found in the food additive E174 used for decoration of pastries and chocolates.^[13] Finally, some unauthorized food supplements claiming to support the immune system contain AgNPs^[13] and their use can lead to an uptake of silver up to 0.02 mg kg⁻¹ body weight per day.^[14]

1. Introduction

Because of their small size and high reactivity, nanomaterials (NMs) acquire unique properties that could be interesting for a large scale of applications.^[1–3] Among them, silver nanoparticles (AgNPs) are found in the highest number of consumer products.^[4] Showing strong antimicrobial properties, they are highly attractive for industrial applications and they have already been incorporated into textiles, cosmetics, medical products, or home appliances.^[5] The agri-food sector appreciates

Besides the consumption of food supplements containing AgNPs, the migration of AgNPs from packaging and containers into food will most probably lead to their ingestion. However, despite the great interest they represent for many applications, their unique properties might cause adverse health effects.^[2] Indeed, some cases of argyria (a bluish-gray pigmentation of skin caused by silver accumulation) have already been described after the uptake of colloidal silver as food supplements.^[15–17] *In vivo* studies might be useful to improve the knowledge about the distribution of AgNPs inside the body. AgNPs can reach the systemic circulation and be distributed in various organs as observed in rats after oral ingestion, with the highest levels found in the gastrointestinal tract (GIT) and in the liver and kidneys.^[18,19]

On their side, *in vitro* studies may provide information about the adverse effects caused by the accumulation of AgNPs in organs.^[20] Even if the complete mechanism of AgNPs toxicity is not yet fully understood,^[21] it has been demonstrated that AgNPs can disturb different targets within the cells.^[22] Indeed, AgNPs might bind to membrane proteins and disturb permeability.^[23] They are also able to enter cells, usually by endocytosis and be dissolved into Ag⁺ in endosomes and lysosomes where prevails an acidic pH. Ag⁺ can thus spread in the whole cell, alter proteins and DNA, and trigger the production of

L. Laloux, D. Kastrati, Prof. Y.-J. Schneider
Louvain Institute of Biomolecular Science and Technology (LIBST)
Université catholique de Louvain (UCLouvain)
Place Croix-du-Sud, 4-5 bte L7.07.03, Louvain-la-Neuve B-1348, Belgium
E-mail: yves-jacques.schneider@uclouvain.be

Dr. S. Cambier, Prof. A. C. Gutleb
Environmental Research and Innovation (ERIN) Department
Luxembourg Institute of Science and Technology (LIST)
Rue du Brill, 41, Belvaux L-4422, Luxembourg
E-mail: arno.gutleb@list.lu

 The ORCID identification number(s) for the author(s) of this article can be found under <https://doi.org/10.1002/smll.201907687>.

DOI: 10.1002/smll.201907687

reactive oxygen species.^[23,24] Oxidative stress might in turn disturb lipids, DNA, proteins, and some organelles, such as mitochondria,^[25] which leads to a decrease of energy production resulting in cell death.^[23,25]

In vitro studies have also been specifically performed on models of the intestinal epithelium to observe the potential effects of AgNPs once they have been ingested. For instance, AgNPs seem to trigger the oxidative stress and a perturbation of cellular metabolism in Caco-2 cells, leading to a decrease of cellular viability.^[26–29] In addition, a modification of cellular morphology^[28,29] and integrity^[30] has been observed upon exposition of these cells to AgNPs.

However, most studies focusing on the impact of AgNPs on intestinal cells were performed with pristine nanoparticles (NPs),^[26–33] i.e., nanoparticles directly purchased from manufacturer or synthesized in the laboratory.^[34] These experiments do not consider their interaction with food components and the potential alterations occurring in the gastrointestinal tract,^[35–37] while it has been shown that AgNPs can be affected by the surrounding conditions.^[38] Due to their high reactivity, NMs might interact with food components, such as carbohydrates, lipids, proteins, and minerals, which may influence their size, charge, agglomeration state, and surface composition.^[35,37,39,40] Besides, once ingested, AgNPs pass through the GIT in which physiological parameters (e.g., pH, ionic strength, protein composition) are constantly evolving and thus influencing the features of AgNPs throughout the digestion process.^[38,41,42] As toxic effects of NMs are related to their physicochemical properties,^[21,43] all the alterations that could take place before AgNPs attain the intestinal cells might affect their potential toxicity^[35,39] and must therefore be included in cytotoxicity investigations to realize an accurate risk assessment.^[37]

The European Food Safety Authority (EFSA) has published a guidance in which recommendations were given for risk assessment of nanomaterials used in the food chain.^[44] EFSA insists on the importance of a correct physicochemical characterization of pristine NMs and after their incorporation in relevant food matrices. Some parameters, such as composition, size, shape, charge, agglomeration state, surface composition should be determined with appropriate techniques and size distribution should be measured with at least two different methods, one of them being electron microscopy. EFSA also highlights the importance of following the fate of nanomaterials in the GIT to determine whether they attain intestinal cells in nanometric form or if they break down during the digestive process.^[44] In vitro models of the GIT might be useful to investigate the alterations of AgNPs in food after ingestion.^[37,38] In addition to escape to ethical restrictions, to be less expensive and more rapid than in vivo studies, in vitro models allow to easily collect a large number of samples, realize various controls, and obtain reproducible results. Even if their approach is clearly reductionist rather than holistic, these models can help to understand the mechanisms and might be useful to regulatory authorities to assess the safety of various compounds.^[9,45,46]

In vitro models of the digestion process have already been used to investigate the fate of AgNPs in the gastrointestinal tract.^[38,41,42,47–51] However, most of them did not take

into account the presence of food components that can also impact their behavior.^[41,42,47,50,51] Two studies have nevertheless characterized the fate of poly(acrylic acid) stabilized ultrasmall AgNPs with a radius around 3 nm in the presence of the major food components, mimicked by the presence of starch, olive oil, and skimmed milk powder during the digestion process but particle size distribution was only analyzed with small-angle X-ray scattering.^[38,48] Another study investigated the behavior of AgNPs incorporated in chicken meat during the digestion process but only single-particle inductive coupled plasma-mass spectrometry was applied.^[49]

Therefore, to comply with the recommendations of EFSA, the present study aimed at developing an in vitro method using different techniques to characterize the modifications occurring to AgNPs in contact with food components and throughout the digestive process. We used a previously published standardized food matrix composed of bovine serum albumin (BSA), starch and glyceryl trioleate to represent, respectively, sources of proteins, carbohydrates, and oil.^[52] AgNPs suspension was integrated into this food matrix and then submitted to an in vitro digestion model simulating the three steps of the GIT, i.e., salivary, gastric, and intestinal conditions, by adapting the pH and duration of incubation, as well as incorporating digestive enzymes to the suspension. Contrary to previous publications,^[38,41,42,47–51] this study also took into account the decrease of oxygen level through the gastrointestinal tract. Indeed, oxygen pressure is progressively reduced in the GIT, going from 21% in swallowed air to about 10% in the stomach and less than 5% in the colon.^[53]

After each step of digestion, samples were collected and used to characterize the AgNPs present in the suspension. As suggested by EFSA,^[44] several physicochemical techniques were simultaneously employed, i.e., i) transmission electron microscopy (TEM) that allowed to obtain details on size distribution, shape, and agglomeration state; ii) nanoparticle tracking analysis (NTA) and dynamic light scattering (DLS) to measure the hydrodynamic diameter of NPs; iii) electrophoretic light scattering (ELS) to determine the charge of AgNPs; and iv) UV–visible (UV–vis) spectroscopy to establish their optical properties. Additionally, the formation of a protein corona during the digestive process was quantified using a biochemical assay.

NM-300K AgNPs were selected to realize this study as they have been extensively characterized and are representative of NMs applied for industrial application and commercial use. Indeed, NM-300K AgNPs are included by the European Commission's Joint Research Centre (JRC) in its Nanomaterials Repository,^[54,55] which contains samples of industrially relevant manufactured nanomaterials obtained by subsampling from a single batch, so that all the vials can be assumed identical. Established in 2009, this repository was initially put in place to support the Working Party on Manufactured Nanomaterials Programme but since then, it has also provided materials to various EU-funded projects, as well as national, international, and industrial initiatives. Therefore, the use of representative manufactured nanomaterials, such as NM-300K AgNPs facilitates the comparison of results obtained by different studies and allows a better reproducibility and reliability by minimizing the variability due to the nanomaterial.^[55]

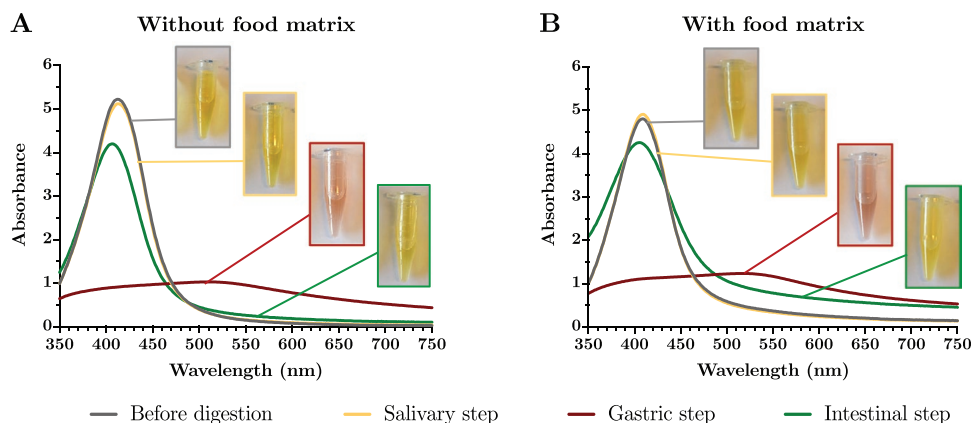


Figure 1. Representative UV–visible absorbance spectra and pictures of AgNPs suspension during in vitro digestion. AgNPs were either A) simply diluted in HBSS or B) incorporated in a standardized food matrix. Gray lines corresponded to AgNPs suspension before digestion, while AgNPs after the salivary, gastric, and intestinal phases were represented with yellow, red, and green lines, respectively.

2. Results

2.1. Properties of AgNPs Before their Incorporation in the Food Matrix

Before incorporating AgNPs suspension in a standardized food matrix and simulating their passage through the GIT, physico-chemical properties of NM-300K AgNPs diluted in Hank's balanced salt solution (HBSS) were monitored. Various techniques were used in parallel. UV–vis spectroscopy allowed to follow the surface plasmon resonance peak (SPR) peak of AgNPs. TEM gave information about the shape, the agglomeration state and the core size of NPs. Besides, the hydrodynamic diameter was established either by NTA or with DLS, while the zeta-potential was determined with ELS. Finally, the protein corona was quantified using the micro-BCA assay.

Before their incorporation in the food matrix, AgNPs suspension was yellow colored with an absorption peak at 412 nm due to the SPR phenomenon (Figure 1A and Table 1, before digestion, without food matrix). As observed in TEM pictures, AgNPs were spherical and well dispersed (Figure 2A). Their mean diameter was around 18.5 nm, while their hydrodynamic diameter varied between 27.4 and 56.8 nm depending on the technique used for its determination. This suspension was slightly negative with a zeta-potential around -10 mV (Table 2, before digestion, without food matrix). Finally, as expected in the absence of proteins in the suspension, no

Table 1. Absorption peak wavelength (λ_{\max} (nm)) during in vitro digestion of AgNPs incorporated or not in a standardized food matrix. Mean values \pm standard deviation were obtained from 4 independent repetitions. Either in the presence or absence of food matrix, letters indicate significant impact of digestion step, with data not connected to the same letter being significantly different from each other ($P < 0.05$). * indicates for each step of digestion, a statistically significant impact of the food matrix ($P < 0.05$).

	Before digestion	Salivary step	Intestinal step
Without food matrix	412 ± 1^a	413 ± 1^a	407 ± 1^b
With food matrix	$408 \pm 1^{*a}$	$409 \pm 1^{*a}$	$405 \pm 1^{*b}$

protein corona was detected around these AgNPs (Figure 3, before digestion, without food matrix).

2.2. Fate of AgNPs in the Presence of Food Components

Alterations of AgNPs suspension appeared after its incorporation into a standardized food matrix composed of starch, BSA, and glyceryl trioleate. Even if AgNPs kept their yellow color (Figure 1B), a significant blueshift of the SPR peak from 412 to 408 nm was recorded (Table 1, with food matrix, before digestion). A significant increase of the hydrodynamic diameter was also induced as observed both with NTA (from 27.4 to 40.2 nm) and DLS (from 56.8 to 247.5 nm). Besides, AgNPs zeta-potential was significantly altered, varying from -9.89 to -5.29 mV (Table 2, with food matrix, before digestion). All these modifications occurred simultaneously with the formation of a protein corona around NPs as emphasized with the micro-BCA quantification (Figure 3, with food matrix, before digestion). However, no modification of the AgNPs core diameter was recorded (Table 2, with food matrix, before digestion). Finally, the shape and the agglomeration state of AgNPs in the presence of food matrix remained also identical to those of initial AgNPs as supported by TEM pictures (Figure 2E).

2.3. Fate of AgNPs During the Salivary Step

To study the fate of AgNPs in the GIT, two kinds of in vitro digestions of AgNPs were performed, either in the presence or absence of a standardized food matrix. After each step of digestion, AgNPs samples were collected and characterized with the same techniques as before.

AgNPs properties were almost not influenced after simulating salivary digestion. Despite a slight difference in the core diameter of nanoparticles measured with TEM micrographs, no difference was recorded in the color and the SPR peak (Figure 1, yellow lines), as well as in the hydrodynamic diameter (Table 2, salivary step), the shape and the agglomeration state (Figure 2B,F) for both AgNPs suspension, i.e., in the absence

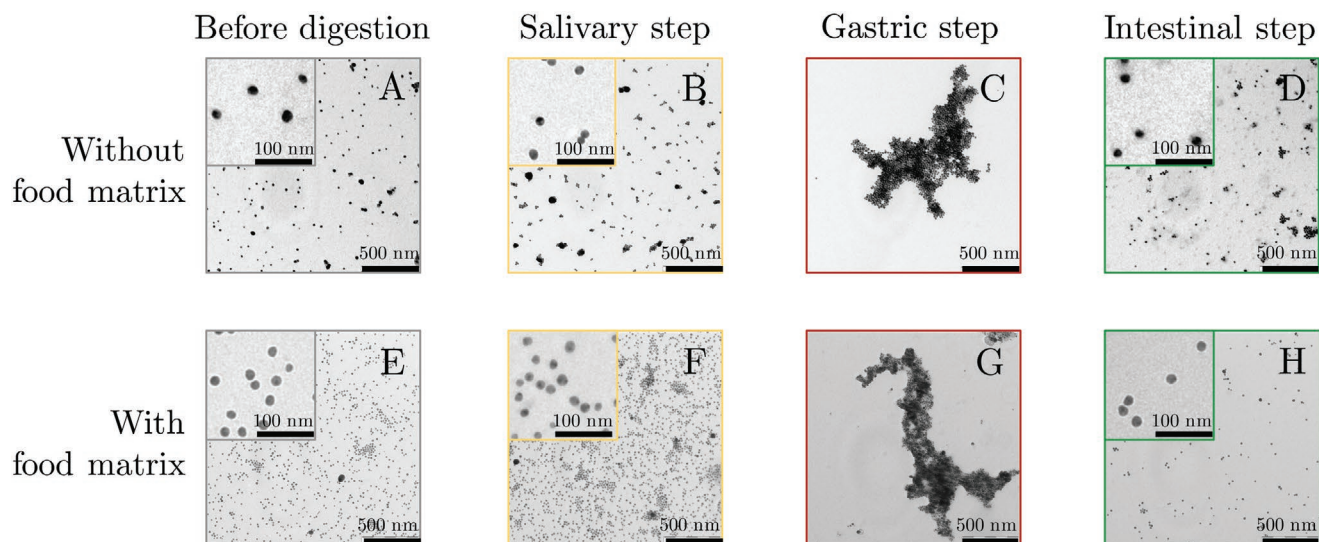


Figure 2. Representative TEM micrographs of AgNPs suspension during in vitro digestion. Micrographs were taken for AgNPs A–D) in the absence or E–H) presence of food components, and A,E) before or after B,F) salivary, C,G) gastric, and D,H) intestinal step of digestion.

and presence of food matrix. The protein corona was also not influenced by the presence of the salivary fluids (Figure 3, yellow bars). Finally, zeta-potential remained around -5 mV in the presence of the food matrix while, in the absence of food matrix, AgNPs were less negative as supported by the zeta-potential that shifted from -9.89 to -6.55 mV (Table 2, salivary step).

Alterations of SPR peak and hydrodynamic diameter due to the presence of food components monitored before digestion were also observed during the salivary step. The protein corona formed with the addition of BSA remained also present after the addition of salivary fluids. Only the zeta-potential was not significantly different anymore due to the modification that occurred for AgNPs charge in the absence of food matrix during this phase.

2.4. Fate of AgNPs During the Gastric Phase

Contrary to the salivary step, the gastric phase highly influenced the fate of AgNPs as observed after the drop of pH and

the addition of pepsin. Indeed, both in the absence and presence of food matrix, AgNPs suspension color turned from yellow to red resulting in a loss of the SPR absorption peak that extended to higher wavelengths (Figure 1, red lines). This change in optical properties was accompanied by the agglomeration of AgNPs as presented in TEM images in Figure 2C,G. These clusters were mainly composed of silver as observed with energy dispersive X-ray spectroscopy (EDX) analysis of AgNPs sample without food matrix (Figure S1, Supporting Information). This agglomeration was also detected with the measurement of the hydrodynamic diameter that drastically increased during the gastric step. For instance, when measured with DLS, it raised from 71.5 nm after the salivary step to 1074.6 nm in the absence of food matrix and from 208.9 to 1342.7 nm in the presence of food components (Table 2, gastric phase). The zeta-potential was also significantly altered during this agglomeration, becoming slightly positive with values of $+1.23$ and $+0.98$ mV, respectively in the absence and presence of food matrix (Table 2, gastric phase). This agglomeration was not only due to the drop of pH but also to the presence of

Table 2. Size and zeta-potential of AgNPs in the presence and absence of food components during each phase of in vitro digestion. Size was determined with TEM, NTA, or DLS while zeta-potential was measured by ELS. Data were presented as mean values \pm standard error of the mean (SEM). Either in the presence or absence of food matrix, letters indicate significant impact of digestion step, with data not connected to the same letter being significantly different from each other ($P < 0.05$). * indicates for each step of digestion, a statistically significant impact of the food matrix ($P < 0.05$).

Food matrix	Digestion step	Diameter by TEM [nm]	Diameter by NTA [nm]	Diameter by DLS [nm]	Zeta-potential [mV]
Without	Undigested	18.57 ± 0.18^a	27.4 ± 0.9^a	56.8 ± 3.9^a	-9.89 ± 1.07^a
	Salivary	18.38 ± 0.14^b	28.6 ± 1.0^a	71.5 ± 7.8^a	-6.55 ± 0.41^b
	Gastric	Agglomerates	87.2 ± 7.9^b	1074.6 ± 47.7^b	$+1.23 \pm 0.15^c$
	Intestinal	17.44 ± 0.06^a	26.5 ± 0.6^a	56.4 ± 0.9^a	-18.64 ± 0.31^d
With	Undigested	14.98 ± 0.03^a	$40.2 \pm 2.6^{*a}$	$247.5 \pm 38.5^{*a}$	$-5.29 \pm 0.28^{*a}$
	Salivary	15.58 ± 0.02^b	$45.1 \pm 4.8^{*a}$	$208.9 \pm 9.0^{*a}$	-5.18 ± 0.61^a
	Gastric	Agglomerates	125.7 ± 13.6^b	$1342.7 \pm 31.2^{*b}$	$+0.98 \pm 0.20^b$
	Intestinal	15.39 ± 0.07^c	$52.2 \pm 8.8^{*a}$	$502.4 \pm 30.0^{*c}$	$-24.89 \pm 0.83^{*c}$

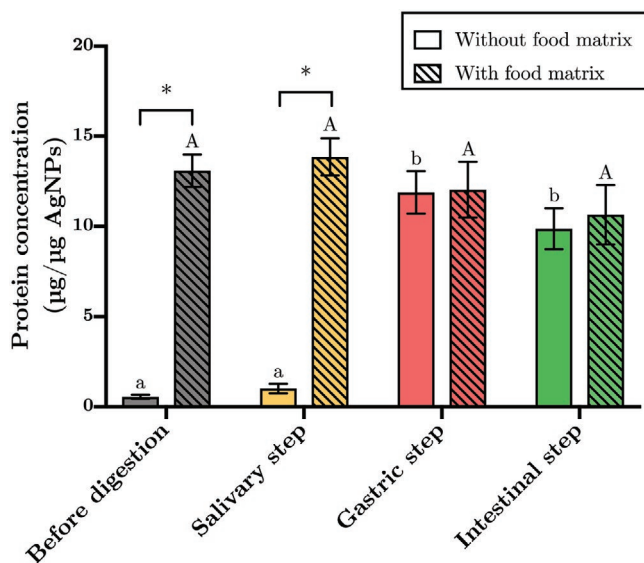


Figure 3. Quantification of protein corona around AgNPs in the presence or absence of food matrix and after each step of in vitro digestion, using micro-BCA assay. Concentrations were given in μg of protein per μg of silver. Mean values \pm SEM were obtained from 3 independent repetitions with three replicates. Either in the presence or absence of food matrix, letters indicate significant impact of digestion step, with data not connected to the same letter being significantly different from each other ($P < 0.05$). * indicates for each step of digestion, a statistically significant impact of the food matrix ($P < 0.05$).

digestive enzymes as AgNPs suspension remained yellow and kept its absorption peak in the absence of digestive enzymes (Figure S2, Supporting Information). Indeed, in the presence of digestive enzymes, a protein corona was formed around AgNPs in the absence of food matrix, while the protein corona already disposed in the presence of food components remained present (Figure 3, red bars).

The effect of food components was hidden during this gastric phase for which few differences in size, shape, agglomeration state, and zeta-potential were observed between AgNPs digested in the presence and absence of food matrix.

2.5. Fate of AgNPs During the Intestinal Step

Major modifications of AgNPs properties also occurred during the intestinal phase. With the pH increase and the addition of bile and pancreatic enzymes, agglomerates formed during the gastric step were disintegrated to recover spherical and dispersed NPs (Figure 2D,H). Following this breakdown, AgNPs suspension retrieved its yellow color and its absorption peak (Figure 1, green lines). However, a significant blueshift of the SPR peak appeared, either in the absence (from 412 nm before digestion to 407 nm) or presence of food components (from 408 to 405 nm) (Table 1, intestinal step). Regarding the size, compared to results obtained before digestion, no modifications were observed for AgNPs in the absence of food matrix during this intestinal phase, while the core diameter and the hydrodynamic diameter measured with DLS increased significantly in the presence of food components (Table 2, intestinal

phase). The protein corona formed earlier was still detected around both types of AgNPs (Figure 3, green bars). This was accompanied by a significant raise of negative charge as zeta-potential of AgNPs attained -18.64 and -24.89 mV, respectively, in the absence and presence of food matrix (Table 2, intestinal step). Finally, the effects of food components that were hidden during the gastric phase were visible again on hydrodynamic diameter and zeta-potential.

3. Discussion

As suggested by EFSA,^[44] the aim of the present study was to monitor the alterations displayed by NM-300K AgNPs once entered in contact with food components and submitted to an in vitro digestive process. Various techniques as TEM, DLS, NTA, and UV-vis spectroscopy were employed to determine the shape, size, agglomeration state, and charge of AgNPs. The presence of a protein corona was also investigated using a biochemical assay. Only one concentration of AgNPs ($675 \mu\text{g mL}^{-1}$) was fully characterized during this study, however, supplementary UV-vis spectroscopy analyses indicated that AgNPs at other concentrations (22.5 and $202.5 \mu\text{g mL}^{-1}$) present the same behavior, suggesting that the observed effects were not dependent of the dose (Figure S3, Supporting Information).

In a first time, physicochemical properties of AgNPs diluted in HBSS were assessed before their incorporation in a food matrix. AgNPs were spherical and well dispersed with a diameter measured by TEM around 18 nm and an absorption peak at 412 nm, which is in accordance with published data.^[54] The zeta-potential was slightly negative, again in agreement with published results for AgNPs dispersed in different media for ecotoxicological testing.^[56] As observed in other studies, the size measured by DLS or NTA was larger than the diameter obtained by TEM.^[47,54,56,57] It can be explained by the difference of measurement principles and the preparation of samples.^[58] Indeed, as sample has to be dried for electron microscopy, the diameter measured by TEM only takes into account the core of the nanoparticle, while NTA and DLS are performed in suspension and measure the hydrodynamic diameter, i.e., the core and the coating. In this study, two dispersing agents were used to stabilize AgNPs and their presence around the nanoparticles is thus comprised in the size measured with DLS and NTA.^[50,59]

Even if DLS and NTA both allow to determine the hydrodynamic diameter, a difference appeared between the two techniques, with NTA providing a smaller size than DLS. DLS determines the size of particles by converting the intensity of the scattered light due to the Brownian movement of the NPs. This technique is highly sensitive to the presence of large particles, which can disturb the measurement and provide a larger size than the expected value.^[59,60] NTA is also based on light scattering but it uses a charge-coupled device (CCD) camera to visualize the nanoparticles individually, the size is thus determined by analyzing the Brownian motion of each particle separately. This technique provides size closer to the real value and can furthermore be very useful in the case of complexed mixture, such as food matrix or digestive fluids.^[58,60] Nevertheless, whereas DLS is very user-friendly, NTA needs several parameters adjustments by a skilled operator, which can

be time-consuming. Besides, NTA requires appropriate concentration of particles, while DLS is adapted to a broad range of concentrations.^[60] In this study, AgNPs suspension had to be diluted between 100- and 2000-fold for NTA measurement, which might have an impact on the hydration layer and alter the size distribution.^[60] Therefore, combining both techniques enables to take into account the drawbacks of each method and allows obtaining a correct size range of the AgNPs hydrodynamic diameter.

After characterizing AgNPs diluted in HBSS, the impact of food components was assessed. TEM images indicated AgNPs remained well dispersed, with the same shape and the same core diameter in the presence of the food matrix. However, an increase of the hydrodynamic diameter was recorded and even if AgNPs suspension kept its yellow color, a blueshift in the SPR peak was noticed. This can be due to the binding of the food components to AgNPs, forming a corona around them.^[61] Food components may stabilize the AgNPs suspension.^[38] In that study, oil and starch have shown similar results but the strongest stabilization was obtained with milk proteins.^[38] A blueshift of the SPR peak of AgNPs has been reported as a result of interaction with BSA, used to mimic the protein source in our study.^[61–63] It has been suggested that this blueshift is due to the replacement of the surfactant (the same as for NM-300K AgNPs) around AgNPs by BSA,^[61] which increases the electron density on the nanoparticle surface and leads to a higher plasmon frequency (thus a lower wavelength).^[61,62] In our study, the formation of a protein corona around AgNPs after the addition of a food matrix was also evidenced after protein quantification with the micro-BCA assay. This method was previously used in other studies^[64–66] and allows to confirm that the alterations of the hydrodynamic diameter, the zeta-potential and the SPR peak of AgNPs in the presence of food components can be attributable to the binding of BSA molecules to the nanoparticles.

During the first stage of digestion, i.e., the oral phase, and in the absence of food matrix, no alteration of the physicochemical properties of the NPs was observed except a decrease of the zeta-potential. As suggested by some studies,^[67,68] the lower negative charge can be explained by the slight pH decrease of the AgNPs suspension, passing from a range of 7.08–7.4 after the dilution in HBSS before digestion to a pH of 6.9 during the salivary step. Neither adsorption of α -amylase nor modification of hydrodynamic diameter were noticed in our study. However, some studies investigating the fate of AgNPs during the salivary digestion observed a slight increase of the hydrodynamic diameter,^[41,42,47,50] suggesting a small agglomeration or the formation of a protein corona. These studies differ from ours in the digestion protocol and the type of AgNPs (size and coating), which can explain the dissimilarity. In the presence of food matrix, AgNPs did not undergo any modification during the oral phase, which is consistent with previous results.^[38]

Unlike the oral phase, the gastric step highly modified the AgNPs properties. Besides the shift to a slight positive zeta-potential, an increase of the hydrodynamic diameter was noticed and can be explained by the agglomeration of AgNPs as observed on TEM images. This is in agreement with other studies that also mentioned the clustering of AgNPs submitted to a gastric digestion.^[36,41,42,47] AgNPs agglomeration was

also detected by UV–vis spectroscopy in line with published results.^[36,47,51] Indeed, UV–vis spectroscopy allows to distinguish dissolution from agglomeration of AgNPs. A dissolution of the nanoparticles is accompanied by a decrease of the absorption peak of AgNPs around 400 nm due to the loss of particles absorbing the light. While the agglomeration causes a reduction of the absorption peak around 400 nm but also an increase of a second broader absorption peak above 500 nm. This is induced by the decrease of AgNPs surface energy, which reduces the plasmon frequency and increases the absorption wavelength.^[51] An agglomeration of AgNPs was also observed in the presence of food components and was again in line with previous observations.^[38]

In the absence of digestive enzymes during the gastric phase, no agglomeration of AgNPs was detected, similar to what has been observed in the past.^[50] Therefore, the presence of digestive enzymes combined to an acidic pH seems essential to trigger NM-300K agglomeration in the stomach. The drop of pH allows the destabilization of the coating and influences the interactions between AgNPs and enzymes, which facilitates the adsorption of enzymes to the NPs and enhances their agglomeration as previously emphasized.^[36,41] The presence of proteins around NPs was confirmed using the micro-BCA assay, which reveals the involvement of proteins in the clustering. These results were in agreement with a previous study that also noticed the formation of a protein corona during the gastric phase by analyzing TEM images.^[42]

According to EDX analysis, only silver was present in agglomerates formed during the gastric phase, which is contrary to other studies that indicated also the presence of chlorine in the clusters.^[50,69–71] Besides the type of coating and size of AgNPs, the digestion protocol differs between our study and these four other ones. First, this study was the only one to take into account the decrease of oxygen level in the stomach and the intestine.^[50,69–71] Indeed, oxygen concentration is gradually lowered in the lumen of the GIT, going from 21% in swallowed air to about 10% in the stomach and less than 5% in the colon.^[53] Therefore, the bottles in which the digestion were performed were flushed with N₂ before the incubation for the gastric step to reduce the oxygen level. A second flushing was also realized before the intestinal step. Second, this study included digestive enzymes, which was not the case for three of the aforementioned studies.^[69–71] All these changes could impact the presence of chlorine in the clusters. Even if the acidic conditions enhance the oxidative dissolution of Ag⁰ into Ag⁺ at the surface of AgNPs, which can lead to the agglomeration of AgNPs due to the formation of AgCl after the binding of Cl[−] of the medium, decreasing the surface charge of the NPs,^[36,69,72] the reduction of oxygen level decreases this dissolution and the formation of Ag⁺.^[73,74] At low silver ion concentration, Ag⁺ preferentially binds to proteins rather than chlorine because of the higher stability of the complexes with sulfhydryl groups.^[51] Therefore, despite the acidic pH and the presence of chlorine in the medium, the decrease of oxygen level could explain the absence of Cl in the Ag clusters, proteins interacting primarily with AgNPs in this case.

Finally, the simulation of the intestinal phase also influenced the AgNPs features. Both in the presence or absence of food components, the pH increase and the addition of bile

and pancreatic enzymes disintegrated the clusters formed during the gastric phase as observed on TEM images. It was accompanied by a recovery of the yellow color and the absorption peak around 410 nm. However, a blueshift of the SPR peak was detected in both cases compared to undigested AgNPs. As already detailed above, this blueshift can be due to the presence of a protein corona around the AgNPs^[61,62] and was confirmed with the micro-BCA assay. Indeed, some studies underlined the ability of digestive enzymes to bind around NPs.^[75–80] Besides, bile salts can also interact with the NPs and complete the corona.^[41,81] This corona stabilizes the NPs as it was emphasized by the raise of negative zeta-potential.^[82] These results were in accordance with an earlier study that also recovered dispersed AgNPs after disintegration of clusters formed during the gastric phase^[50] and a second one that reported TEM micrographs with dispersed AgNPs surrounded by a protein corona after the intestinal step.^[51] Food components also influence the fate of AgNPs as their presence increased the zeta-potential as well as the diameter of the AgNPs. Some studies suggest that these components as well as peptides, oligosaccharides or fatty acids formed after their digestion could bind to AgNPs and act as an additional stabilizer of the NPs suspension.^[38,48] In this study, we needed to reduce the starch concentration compared to the EU recommendation to obtain a better dissolution. The presence of additional starch and oligosaccharides could increase the stabilization of AgNPs already observed in intestinal fluids. Some studies indeed demonstrated that starch and other carbohydrates can bind to nanoparticles and take part in the corona formation.^[35,83,84] However, it was previously suggested that proteins of the food matrix have stronger stabilizing properties than carbohydrates and fat,^[38] so that we could assume that the digestive enzymes and the protein fraction of the food matrix are mainly responsible of the stabilization of AgNPs observed during the simulation of intestinal digestion.

In this study, the choice of a standardized food matrix representing the three major sources of nutrients was made as it would be difficult to represent all the diversity of eating habits. In addition, even if an *in vitro* model of digestion cannot perfectly reflect reality since the composition of the digestive system can vary from one person to another, or even from one meal to another, this study tried to get as close to physiological conditions as possible by mimicking food and taking into account variations in pH and oxygen level within the GIT, as well as using the main enzymes encountered throughout the digestion process. Altogether, the results of this study indicate that AgNPs might reach the intestinal epithelium in nanometric form but with alterations of their properties and the formation of a protein corona. This might in turn influence their future toxicity and fate inside the body.^[35,39] This study confirms the importance of considering the behavior of AgNPs within the digestive system before carrying out toxicity studies on the intestinal epithelium.^[44] Finally, this protocol could easily be used with other nanomaterials and allow the comparison of the fate of different types of nanomaterials in the GIT. Indeed, the properties of various ingested NMs might be considerably different and influence their fate in the GIT.^[37] For instance, the formation of the protein corona can vary for different NMs as the elemental composition but also the size, the charge, the surface properties or the coating of a NM can

influence the binding of proteins.^[37,85–88] This method could be used for a larger screening of the fate of NMs in the GIT and might be useful to assist regulatory authorities in their decision making regarding the risk assessment of nanomaterials.^[37,44]

4. Conclusion

In this study, the impact of the food components and the gastrointestinal fluids on the properties of NM-300K AgNPs was investigated. Food components were found to form a corona around the NPs, while the gastrointestinal fluids highly influenced the fate of AgNPs. Even if minor change was observed during the salivary phase, the simulation of the gastric phase triggered the agglomeration of AgNPs forming clusters with proteins. The passage to the intestinal phase then disintegrated these clusters, correctly dispersed AgNPs were recovered but the presence of a corona around the NPs was emphasized with the various used techniques. To conclude, all these modifications indicated that intestinal cells do not encounter pristine AgNPs, which must be taken into account to realize an accurate risk assessment of ingested AgNPs. Further studies are needed to investigate the effects of these modified AgNPs on intestinal cells.

5. Experimental Section

Silver Nanoparticles: The experiments were performed with NM-300K silver nanoparticles purchased from the Fraunhofer Institute for Molecular Biology and Applied Ecology (Schmallenberg, DE). NM-300K is a yellow-brown colloidal dispersion of AgNPs containing 10.16% (w w⁻¹) of silver dispersed in water with stabilizing agents consisting of 4% (w w⁻¹) each of polyoxyethylene glycerol trioleate and polyoxyethylene (20) sorbitan mono-laurate (Tween 20). The NM-300K suspension was characterized by the JRC repository, Ispra, IT) and contains silver particles with a mean diameter of 15 nm with a narrow size distribution of 99% of the particles having a diameter below 20 nm. A second restricted population of 5 nm was also identified by TEM.^[54,89] For the experiments, AgNPs were added to HBSS (Lonza, Verviers, BE) or the standard food matrix to reach a concentration of 67.5 µg mL⁻¹.

Food Matrix and Digestive Enzymes: Three standard macronutrients previously selected and tested^[52] were used to model the food matrix. BSA (lyophilized powder, A4503, >96%, Sigma-Aldrich, Saint-Louis, MO) was used for the protein fraction, glyceryl trioleate (glyceryl trioleate, T7140, >99 %, Sigma-Aldrich) stood for the lipid fraction, and carbohydrates were simulated by starch (unmodified wheat starch, S5127, Sigma-Aldrich). The concentrations were calculated to represent concentrations found at the intestinal level by taking into account the volumes of ingested and secreted fluids together with the relative proportions of the major dietary nutrients. In 24 h, people drink ≈2 L and secrete ≈7 L of gastrointestinal fluids (i.e., 1 L of saliva, 2 L of gastric juice, 1 L of bile, 2 L of pancreatic juice, and 1 L of intestinal juice).^[52] According to the EU regulation No. 1169/2011 on the provision of food information to consumers, macronutrients reference intakes are ≈50 g of proteins, ≈260 g of carbohydrates, and ≈70 g of fats leading to a concentration of ≈5.6 g L⁻¹ of BSA, 28.9 g L⁻¹ of starch, and 7.8 g L⁻¹ of glyceryl trioleate.^[90] The starch concentration was however reduced to 8.7 g L⁻¹ to allow a better dissolution. The standardized food matrix was prepared by mixing the three major nutrients in HBSS to reach the desired concentration.

The different digestive enzymes and bile extract were obtained from Sigma-Aldrich. A stock solution of α-amylase from human saliva (type IX-A, A0521, 160 units mg⁻¹ solid, 1 880 units mg⁻¹ protein) was prepared

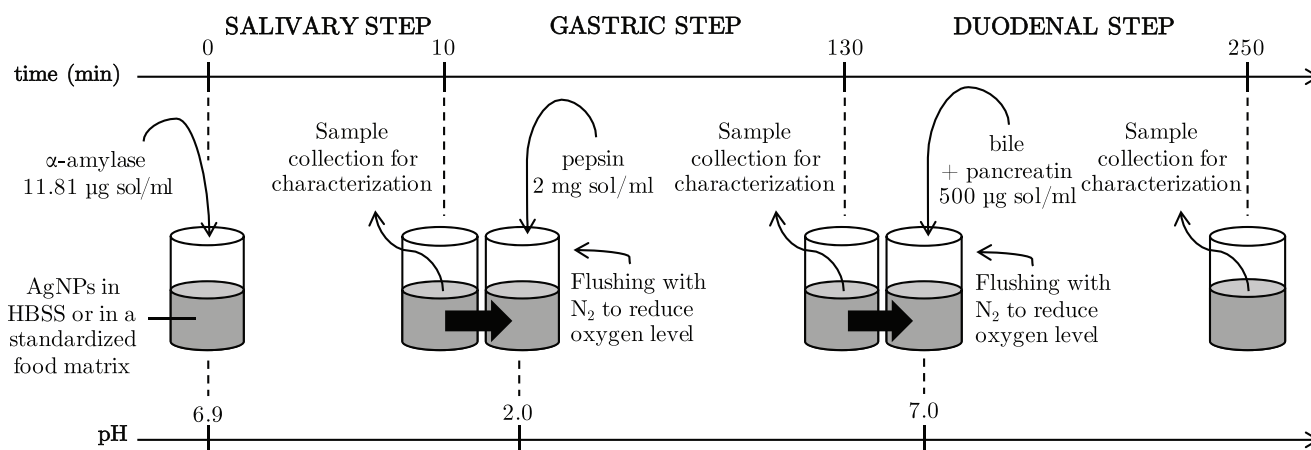


Figure 4. Schematic overview of the in vitro digestion protocol.

in the phosphate-buffered saline solution to reach a concentration of $166.67 \text{ units mL}^{-1}$ and stored at -20°C until use. For each experiment, a solution of porcine pepsin from gastric mucosa (P7000, $561 \text{ units mg}^{-1}$ solid) at 0.04 g mL^{-1} in 0.1 M HCl was freshly prepared as well as a mixture of pancreatin from porcine pancreas (P1750, activity equivalent to $4 \times \text{USP specifications}$) and porcine bile extract (B8631), both at 3.3 mg mL^{-1} in 0.1 M NaHCO_3 . Pancreatin is composed of several pancreatic enzymes, such as α -amylase, lipase, colipase, ribonuclease, trypsin, and other proteases, while bile extract contains various bile salts including glycine and taurine conjugates of hyodeoxycholic acid.

Precolonic In Vitro Digestion: The precolonic in vitro digestion protocol was adapted from^[52] and is summarized in **Figure 4**. AgNPs resuspended by vortexing in HBSS or in the standardized food matrix were incubated in 25 mL amber bottles at 37°C , with a constant magnetic stirring of 350 rpm. For the salivary step, the pH was adjusted to 6.9 with 1 M HCl and 11.8 µg of solid α -amylase were added per mL of digesting solution for 10 min. The pH was decreased to 2.0 for the gastric step by adding 1 M HCl and pepsin was incorporated to the digesting solution to reach $2 \text{ mg solid mL}^{-1}$. After 2 h of incubation, the pH was increased to 5.3 with 1 M NaHCO_3 to initiate the duodenal step. The mixture containing pancreatin and bile extract at ratio 1:1 was added to the digesting solution to attain $0.5 \text{ mg solid mL}^{-1}$ of each. The pH was then adjusted to 7.0 with 1 M NaHCO_3 or 1 M HCl and the solution was incubated during 2 more hours. For the gastric and duodenal steps, bottles were flushed by N_2 during 30 s after the adaption of pH and the addition of digestive enzymes. It allows to decrease the level of oxygen as occurring in the stomach and intestine. After each step of digestion, samples were collected and used to characterize the AgNPs.

UV-Vis Spectroscopy: Modifications of AgNPs suspension during the digestion process were carried out using UV-vis spectroscopy. The absorbance spectrum of AgNPs samples was recorded with a Genesys 10S UV-vis spectrophotometer (Thermo Scientific, Waltham, MA) in the wavelength range of 350–750 nm. HBSS was used as blank and all AgNPs suspensions except those obtained after the gastric step were diluted three times in HBSS immediately before the analysis. Four independent experiments were performed. UV-vis spectroscopy analyses were also performed with other concentrations of AgNPs (22.5 and 202.5 µg mL^{-1}) submitted to the digestion process to confirm that the observed effects were not dependent of the dose (Figure S3, Supporting Information).

Transmission Electron Microscopy: Transmission electron microscopy was used to visualize the size, shape, and agglomeration state of AgNPs before digestion and after each step of the digestive process. AgNPs suspension were first concentrated by centrifugation to have enough particles to cover the grid used for the TEM imaging. In the absence of food matrix, undigested AgNPs and those collected after the salivary step were centrifuged at $14\,000 \text{ g}$ for 40 min. AgNPs from gastric step were centrifuged at 1500 g during 5 min and those from the intestinal step were submitted to a centrifugation of $10\,000 \text{ g}$ for 40 min. In the

presence of food matrix, 3 centrifugations of 1 min at 2000 g were first performed to remove the excess of starch for undigested AgNPs and those collected after the salivary and the intestinal steps. Then, they were centrifuged at 6000 g for 1 h to collect a pellet of AgNPs. AgNPs from the gastric step were three times centrifuged at 200 g during 1 min to remove the excess of starch and then at 750 g during 5 min to collect the AgNPs pellet.

Each pellet was then placed on a carbon-coated 200 mesh copper grid (CF200-Cu, Electron Microscopy Science, Hatfield, PA) for 10 min. The grid was rinsed with water and finally dried with a filter paper. All grids except for the gastric step were pretreated with 1% (w v^{-1}) Alcian Blue (Sigma-Aldrich) for 10 min to enhance AgNPs attachment on the grid by introducing positive charges.^[91] Grids were analyzed with a LEO922 transmission electron microscope (Zeiss, Jena, DE) and micrographs were recorded using a CCD camera. Particles diameter was obtained from TEM images using ImageJ software (version 1.52a). Three independent experiments were carried out and results are expressed as a mean of all the measured diameters. To determine the elemental composition of the samples, EDX analysis was also realized.

Dynamic and Electrophoretic Light Scattering: Size and zeta-potential of AgNPs were obtained by DLS and ELS using a Zetasizer Nano Series instrument (Malvern Instruments Ltd, UK) with a scattering angle of 173° . The number of runs and their duration were automatically determined by the device. Each sample was measured in three replicates. Results are presented either as a mean of the z-average coming from two independent experiments or as an average of the zeta-potential obtained from three independent tests.

Nanoparticle Tracking Analysis: Nanoparticle tracking analysis was used to measure the hydrodynamic diameter of AgNPs during the digestion process. Before analysis, undigested AgNPs as well as samples from the saliva and intestinal steps were diluted with milli-Q water 2000 times, while samples coming from the gastric step were diluted 100-fold to reach a concentration in the range of 10^8 – $10^9 \text{ particles mL}^{-1}$. Three videos of 60 s were recorded for each sample with the NanoSight instrument (Malvern Instrument Ltd) and analyzed using the NTA 3.2 software. Results are expressed as an average of the modes coming from three independent experiments. The background noise was also obtained from samples containing food components and the different digestive fluids without AgNPs in order to ensure that the scattered light peak measured in the samples containing AgNPs are caused by the nanoparticles (data not shown).

Protein Corona Quantification by Micro-BCA Assay: A micro-BCA assay was performed to reveal the presence of a protein corona around AgNPs incorporated into a food matrix or submitted to the digestion process. First, AgNPs samples were centrifuged with the same parameters than before the TEM grid preparation. The supernatants were removed and the pellets were resuspended by vortexing in milli-Q water. A second centrifugation was performed to get rid of most unbound proteins and

the pellets containing AgNPs with their protein corona were retrieved. Samples with food matrix and digestive enzymes in the absence of AgNPs underwent the same centrifugation steps and served as control.

A micro-BCA assay was then realized to quantify the protein corona (Pierce Micro BCA Protein Assay Kit, Thermo Scientific) following an adaptation of a published method.^[92] Briefly, standards were prepared with known concentrations of BSA. 400 μ L of working reagent were added in microtubes containing 30 μ L of each standard or sample pellet before incubation at 60 °C for 1 h. Microtubes were centrifuged at 14 000 g during 20 min to pellet NPs and 50 μ L of each supernatant was transferred into 96-wells plate (Corning incorporated, Corning, NY) to read absorbance at 562 nm.

Statistical Analyses: Statistical analyses were carried out with R software (version 3.5.0). The *lme* function of the *nlme* package was used to fit linear mixed-effects models taking into account that samples from different steps of digestion were dependent. To fulfil the residuals normality hypothesis, an inverse transformation was applied to the data coming from the NTA, while log and square root transformations were realized on the diameters measured, respectively, by TEM and DLS. The within-group heteroscedasticity structure is taking into account in the *lme* function specifications.^[93] Desired comparisons were conducted with the contrast function of the package with the same name.^[94] Obtained *P*-values were corrected following the Holm method with the *p.adjust* function. For all statistical tests, results were considered significant at the level $\alpha = 0.05$.

Supporting Information

Supporting Information is available from the Wiley Online Library or from the author.

Acknowledgements

The authors would like to thank Pascale Lipnik (UCLouvain) for the training to the use of the transmission electron microscope. They are also grateful to Vincent Bremhorst and Catherine Rasse of the SMCS platform from UCLouvain for the statistical support. This work was financially supported by UCLouvain (FSR grant) and the Association Luxembourgeoise des Amis de la Fondation Louvain (ALAF).

Conflict of Interest

The authors declare no conflict of interest.

Keywords

characterization, food matrix, in vitro digestion, physicochemical properties, silver nanoparticles

Received: December 31, 2019

Revised: February 19, 2020

Published online:

[1] P. N. Sudha, K. Sangeetha, K. Vijayalakshmi, A. Barhoum, in *Emerging Applications of Nanoparticles and Architecture Nanostructures: Current Prospects and Future Trends* (Eds: A. S. H. Makhlof, A. Barhoum), Elsevier, Amsterdam, Netherlands **2018**, Ch. 12.

[2] G. Oberdörster, A. Maynard, K. Donaldson, V. Castranova, J. Fitzpatrick, K. Ausman, J. Carter, B. Karn, W. Kreyling, D. Lai,

S. Olin, N. Monteiro-Riviere, D. Warheit, H. Yang, *Part. Fibre Toxicol.* **2005**, *2*, 8.

- [3] C. Buzea, I. I. Pacheco, K. Robbie, *Biointerphases* **2007**, *2*, MR17.
- [4] The project on emerging nanotechnologies, Consumer products inventory, <http://www.nanotechproject.org/cpi> (accessed: June 2019).
- [5] S. W. Wijnhoven, W. J. Peijnenburg, C. A. Herberts, W. I. Hagens, A. G. Oomen, E. H. Heugens, B. Roszek, J. Bisschops, I. Gosens, D. Van De Meent, S. Dekkers, W. H. De Jong, M. Van Zijverden, A. J. Sips, R. E. Geertsma, *Nanotoxicology* **2009**, *3*, 109.
- [6] M. Rai, S. Deshmukh, A. Ingle, A. Gade, *J. Appl. Microbiol.* **2012**, *112*, 841.
- [7] S. Deshmukh, S. Patil, S. Mullani, S. Delekar, *Mater. Sci. Eng., C* **2019**, *97*, 954.
- [8] Q. Chaudhry, M. Scotter, J. Blackburn, B. Ross, A. Boxall, L. Castle, R. Aitken, R. Watkins, *Food Addit. Contam., Part A* **2008**, *25*, 241.
- [9] L. Laloux, M. Polet, Y.-J. Schneider, in *Nanotechnology in Agriculture and Food Science* (Eds: M. A. Axelos, M. Van de Voorde), Wiley-VCH, Weinheim, Germany **2017**, Ch. 18.
- [10] A. Emamifar, M. Kadivar, M. Shahedi, S. Soleimani-Zad, *Food Control* **2011**, *22*, 408.
- [11] Y. Echevoyen, C. Nerin, *Food Chem. Toxicol.* **2013**, *62*, 16.
- [12] N. von Goetz, L. Fabricius, R. Glaus, V. Weitbrecht, D. Günther, K. Hungerbühler, *Food Addit. Contam., Part A* **2013**, *30*, 612.
- [13] E. Verleysen, E. Van Doren, N. Waegeneers, P.-J. De Temmerman, M. Abi Daoud Francisco, J. Mast, *J. Agric. Food Chem.* **2015**, *63*, 3570.
- [14] P. Larsen, F. Christensen, K. Jensen, A. Brinch, S. Mikkelsen, *Exposure Assessment of Nanomaterials in Consumer Products*, Danish Environmental Protection Agency, Copenhagen, Denmark **2015**.
- [15] L. P. Bowden, M. C. Royer, J. R. Hallman, M. Lewin-Smith, G. P. Lupton, *J. Cutaneous Pathol.* **2011**, *38*, 832.
- [16] A. L. S. Chang, V. Khosravi, B. Egbert, *J. Cutaneous Pathol.* **2006**, *33*, 809.
- [17] I. Jung, E.-J. Joo, B. S. Suh, C.-B. Ham, J.-M. Han, Y.-G. Kim, J.-S. Yeom, J.-Y. Choi, J.-H. Park, *Ann. Occup. Environ. Med.* **2017**, *29*, 45.
- [18] K. Loeschner, N. Hadrup, K. Qvortrup, A. Larsen, X. Gao, U. Vogel, A. Mortensen, H. R. Lam, E. H. Larsen, *Part. Fibre Toxicol.* **2011**, *8*, 18.
- [19] Y. S. Kim, J. S. Kim, H. S. Cho, D. S. Rha, J. M. Kim, J. D. Park, B. S. Choi, R. Lim, H. K. Chang, Y. H. Chung, I. H. Kwon, J. Jeong, B. S. Han, I. J. Yu, *Inhalation Toxicol.* **2008**, *20*, 575.
- [20] H. J. Johnston, G. Hutchison, F. M. Christensen, S. Peters, S. Hankin, V. Stone, *Crit. Rev. Toxicol.* **2010**, *40*, 328.
- [21] M. Akter, M. T. Sikder, M. M. Rahman, A. A. Ullah, K. F. B. Hossain, S. Banik, T. Hosokawa, T. Saito, M. Kurasaki, *J. Adv. Res.* **2018**, *9*, 1.
- [22] P. Asharani, M. P. Hande, S. Valiyaveetil, *BMC Cell Biol.* **2009**, *10*, 65.
- [23] D. McShan, P. C. Ray, H. Yu, *J. Food Drug Anal.* **2014**, *22*, 116.
- [24] V. De Matteis, M. A. Malvindi, A. Galeone, V. Brunetti, E. De Luca, S. Kote, P. Kshirsagar, S. Sabella, G. Bardi, P. P. Pompa, *Nanomed.: Nanotechnol., Biol. Med.* **2015**, *11*, 731.
- [25] L. Z. Flores-López, H. Espinoza-Gómez, R. Somanathan, *J. Appl. Toxicol.* **2019**, *39*, 16.
- [26] A. Martirosyan, K. Grintzalis, M. Polet, L. Laloux, Y.-J. Schneider, *Toxicol. Lett.* **2016**, *253*, 36.
- [27] S. Aueviriyavit, D. Phummiratch, R. Maniratanachote, *Toxicol. Lett.* **2014**, *224*, 73.
- [28] S. Gioria, P. Urbán, M. Hajduch, P. Barboro, N. Cabaleiro, R. La Spina, H. Chassaigne, *Toxicol. In Vitro* **2018**, *50*, 347.
- [29] L. Böhmert, B. Niemann, D. Lichtenstein, S. Juling, A. Lampen, *Nanotoxicology* **2015**, *9*, 852.
- [30] A. Martirosyan, M. Polet, A. Bazes, T. Sergent, Y.-J. Schneider, in *Inflammatory Bowel Disease* (Ed: I. Szabo), IntechOpen, Rijeka, Croatia **2012**, Ch. 8.

- [31] H. Bouwmeester, J. Poortman, R. J. Peters, E. Wijma, E. Kramer, S. Makama, K. Puspitaninganindita, H. J. Marvin, A. A. Peijnenburg, P. J. Hendriksen, *ACS Nano* **2011**, *5*, 4091.
- [32] S. C. Sahu, J. Zheng, L. Graham, L. Chen, J. Ihrle, J. J. Yourick, R. L. Sprando, *J. Appl. Toxicol.* **2014**, *34*, 1155.
- [33] A. Georgantzopoulou, T. Serchi, S. Cambier, C. C. Leclercq, J. Renaut, J. Shao, M. Kruszewski, E. Lentzen, P. Grysan, S. Eswara, J.-N. Audinot, S. Contal, J. Ziebel, C. Guignard, L. Hoffmann, A. J. Murk, A. C. Gutleb, *Part. Fibre Toxicol.* **2016**, *13*, 9.
- [34] D. J. McClements, H. Xiao, P. Demokritou, *Adv. Colloid Interface Sci.* **2017**, *246*, 165.
- [35] M.-R. Go, S.-H. Bae, H.-J. Kim, J. Yu, S.-J. Choi, *Front. Microbiol.* **2017**, *8*, 1.
- [36] A. P. Ault, D. I. Stark, J. L. Axson, J. N. Keeney, A. D. Maynard, I. L. Bergin, M. A. Philbert, *Environ. Sci.: Nano* **2016**, *3*, 1510.
- [37] D. J. McClements, G. DeLoid, G. Pyrgiotakis, J. A. Shatkin, H. Xiao, P. Demokritou, *NanoImpact* **2016**, *3–4*, 47.
- [38] C. Kästner, D. Lichtenstein, A. Lampen, A. F. Thünemann, *Colloids Surf. A* **2017**, *526*, 76.
- [39] Z. Zhang, R. Zhang, H. Xiao, K. Bhattacharya, D. Bitounis, P. Demokritou, D. J. McClements, *NanoImpact* **2019**, *13*, 13.
- [40] A. Dudkiewicz, K. Tiede, K. Loeschner, L. H. S. Jensen, E. Jensen, R. Wierzbicki, A. Boxall, K. Molhave, *TrAC, Trends Anal. Chem.* **2011**, *30*, 28.
- [41] L. Böhmert, M. Girod, U. Hansen, R. Maul, P. Knappe, B. Niemann, S. M. Weidner, A. F. Thünemann, A. Lampen, *Nanotoxicology* **2014**, *8*, 631.
- [42] L. Pindáková, V. Kašpárková, K. Kejlová, M. Dvořáková, D. Krsek, D. Jírová, L. Kašparová, *Int. J. Pharm.* **2017**, *527*, 12.
- [43] M. A. Gattoo, S. Naseem, M. Y. Arfat, A. Mahmood Dar, K. Qasim, S. Zubair, *Biomed. Res. Int.* **2014**, *2014*, 1.
- [44] A. Hardy, D. Benford, T. Halldorsson, M. J. Jeger, H. K. Knutsen, S. More, H. Naegeli, H. Noteborn, C. Ockleford, A. Ricci, G. Rychen, J. R. Schlatter, V. Silano, R. Solecki, D. Turck, M. Younes, Q. Chaudhry, F. Cubadda, D. Gott, A. Oomen, S. Weigel, M. Karamitrou, R. Schoonjans, A. Mortensen, *EFSA J.* **2018**, *16*, 1.
- [45] M. Minekus, M. Alminger, P. Alvito, S. Ballance, T. Bohn, C. Bourlieu, F. Carriere, R. Boutrou, M. Corredig, D. Dupont, C. Dufour, L. Egger, M. Golding, S. Karakaya, B. Kirkhus, S. Le Feunteun, U. Lesmes, A. Macierzanka, A. Mackie, S. Marze, D. J. McClements, O. Ménard, I. Recio, C. N. Santos, R. P. Singh, G. E. Vegarud, M. S. J. Wickham, W. Weitschies, A. Brodtkorb, *Food Funct.* **2014**, *5*, 1113.
- [46] Committee on the Framework for Evaluating the Safety of the Dietary Supplements, Institute of Medicine, National Research Council, *Dietary Supplements: A Framework for Evaluating Safety*, National Academies Press, Washington, DC **2004**.
- [47] P. Bove, M. A. Malvindi, S. S. Kote, R. Bertorelli, M. Summa, S. Sabella, *Nanoscale* **2017**, *9*, 6315.
- [48] D. Lichtenstein, J. Ebmeyer, P. Knappe, S. Juling, L. Böhmert, S. Selve, B. Niemann, A. Braeuning, A. F. Thünemann, A. Lampen, *Biol. Chem.* **2015**, *396*, 1255.
- [49] K. Ramos, L. Ramos, M. Gomez-Gomez, *Food Chem.* **2017**, *221*, 822.
- [50] A. P. Walczak, R. Fokkink, R. Peters, P. Tromp, Z. E. H. Rivera, I. M. Rietjens, P. J. Hendriksen, H. Bouwmeester, *Nanotoxicology* **2012**, *7*, 1198.
- [51] W. Wu, R. Zhang, D. J. McClements, B. Chefetz, T. Polubesova, B. Xing, *Environ. Sci. Technol.* **2018**, *52*, 8792.
- [52] S. Hollebeeck, F. Borlon, Y.-J. Schneider, Y. Larondelle, H. Rogez, *Food Chem.* **2013**, *138*, 1936.
- [53] Y. Bonnet, J. Haberer, R. Schutz, R. Simon, B. Vanwysberghe, R. Mercier, *Ann. Fr. Anesth. Reanim.* **1983**, *2*, 431.
- [54] C. Klein, S. Comero, B. Stahlmecke, J. Romazanov, T. Kuhlbusch, E. Van Doren, P.-J. De Temmerman, J. Mast, P. Wick, H. Krug, G. Locoro, K. Hund-Rinke, W. Kördel, S. Friedrichs, G. Maier, J. Werner, T. Linsinger, B. M. Gawlik, *NM-300 Silver Characterisation, Stability, Homogeneity*, JRC Scientific and Technical Reports, European Union **2011**.
- [55] S. Totaro, G. Cotogno, K. Rasmussen, F. Pianella, M. Roncaglia, H. Olsson, J. M. R. Sintes, H. P. Crutzen, *Regul. Toxicol. Pharmacol.* **2016**, *81*, 334.
- [56] J. Köser, M. Engelke, M. Hoppe, A. Nogowski, J. Filser, J. Thöming, *Environ. Sci.: Nano* **2017**, *4*, 1470.
- [57] M. Connolly, M.-L. Fernandez-Cruz, A. Quesada-Garcia, L. Alte, H. Segner, J. Navas, *Int. J. Environ. Res. Public Health* **2015**, *12*, 5386.
- [58] B. Reidy, A. Haase, A. Luch, K. A. Dawson, I. Lynch, *Materials* **2013**, *6*, 2295.
- [59] M. van der Zande, R. J. Vandebriel, E. Van Doren, E. Kramer, Z. Herrera Rivera, C. S. Serrano-Rojero, E. R. Gremmer, J. Mast, R. J. Peters, P. C. Hollman, P. J. Hendriksen, H. J. Marvin, A. A. Peijnenburg, H. Bouwmeester, *ACS Nano* **2012**, *6*, 7427.
- [60] V. Filipe, A. Hawe, W. Jiskoot, *Pharm. Res.* **2010**, *27*, 796.
- [61] A. Burcza, V. Gräf, E. Walz, R. Greiner, *J. Nanopart. Res.* **2015**, *17*, 428.
- [62] A. Ravindran, A. Singh, A. M. Raichur, N. Chandrasekaran, A. Mukherjee, *Colloids Surf., B* **2010**, *76*, 32.
- [63] G. Wang, Y. Lu, H. Hou, Y. Liu, *RSC Adv.* **2017**, *7*, 9393.
- [64] K. Abstiens, S. M. Figueroa, M. Gregoritz, A. M. Goepferich, *Soft Matter* **2019**, *15*, 709.
- [65] K. Zarschler, K. Prapainop, E. Mahon, L. Rocks, M. Bramini, P. Kelly, H. Stephan, K. Dawson, *Nanoscale* **2014**, *6*, 6046.
- [66] M. S. Grunér, U. Kauscher, M. Linder, M. Monopoli, *J. Proteomics* **2016**, *137*, 52.
- [67] V. R. Chelli, S. S. Bag, A. K. Golder, *Environ. Prog. Sustainable Energy* **2017**, *36*, 192.
- [68] S. P. Dubey, M. Lahtinen, M. Sillanpää, *Colloids Surf. A* **2010**, *364*, 34.
- [69] J. L. Axson, D. I. Stark, A. L. Bondy, S. S. Capracotta, A. D. Maynard, M. A. Philbert, I. L. Bergin, A. P. Ault, *J. Phys. Chem. C* **2015**, *119*, 20632.
- [70] S. K. Mwilu, A. M. El Badawy, K. Bradham, C. Nelson, D. Thomas, K. G. Scheckel, T. Tolaymat, L. Ma, K. R. Rogers, *Sci. Total Environ.* **2013**, *447*, 90.
- [71] K. R. Rogers, K. Bradham, T. Tolaymat, D. J. Thomas, T. Hartmann, L. Ma, A. Williams, *Sci. Total Environ.* **2012**, *420*, 334.
- [72] M. Marchioni, P.-H. Jouneau, M. Chevallet, I. Michaud-Soret, A. Deniaud, *Coord. Chem. Rev.* **2018**, *364*, 118.
- [73] K. Ngamchuea, C. Batchelor-McAuley, R. G. Compton, *Nanotoxicology* **2018**, *12*, 305.
- [74] K. Loza, J. Diendorf, C. Sengstock, L. Ruiz-Gonzalez, J. Gonzalez-Calbet, M. Vallet-Regi, M. Köller, M. Epple, *J. Mater. Chem. B* **2014**, *2*, 1634.
- [75] V. Ernest, G. Sekar, A. Mukherjee, N. Chandrasekaran, *J. Lumin.* **2014**, *146*, 263.
- [76] Y. Ren, J. G. Rivera, L. He, H. Kulkarni, D.-K. Lee, P. B. Messersmith, *BMC Biotechnol.* **2011**, *11*, 63.
- [77] K. Saware, R. M. Aurade, P. Kamala Jayanthi, V. Abbaraju, *J. Nanopart.* **2015**, *2015*, 1.
- [78] M. Nidhin, D. Ghosh, H. Yadav, N. Yadav, S. Majumder, *Mater. Sci. Eng., B* **2015**, *202*, 46.
- [79] A. Gole, C. Dash, V. Ramakrishnan, S. Sainkar, A. Mandale, M. Rao, M. Sastry, *Langmuir* **2001**, *17*, 1674.
- [80] C. Zhang, X. Dong, Z. Guo, Y. Sun, *J. Colloid Interface Sci.* **2018**, *519*, 145.
- [81] T. Winuprasith, S. Chantarak, M. Suphantharika, L. He, D. J. McClements, *J. Colloid Interface Sci.* **2014**, *426*, 333.
- [82] M. Larsson, A. Hill, J. Duffy, *Annu. Trans. – Nord. Rheol. Soc.* **2012**, *20*, 209.
- [83] D. C. Kennedy, G. Orts-Gil, C.-H. Lai, L. Müller, A. Haase, A. Luch, P. H. Seeberger, *J. Nanobiotechnol.* **2014**, *12*, 59.

- [84] A. Amirasr, G. Emtiazi, S. Abasi, M. Yaaghoobi, *J. Biochem. Technol.* **2012**, 3, 280.
- [85] P. Aggarwal, J. B. Hall, C. B. McLeland, M. A. Dobrovolskaia, S. E. McNeil, *Adv. Drug Delivery Rev.* **2009**, 61, 428.
- [86] C. D. Walkey, J. B. Olsen, H. Guo, A. Emili, W. C. Chan, *J. Am. Chem. Soc.* **2012**, 134, 2139.
- [87] L. Treuel, M. Malissek, S. Grass, J. Diendorf, D. Mahl, W. Meyer-Zaika, M. Epple, *J. Nanopart. Res.* **2012**, 14, 1102.
- [88] S. Tenzer, D. Docter, S. Rosfa, A. Wlodarski, J. Kuharev, A. Reik, S. K. Knauer, C. Bantz, T. Nawroth, C. Bier, J. Sirirattanapan, W. Mann, L. Treuel, R. Zellner, M. Maskos, H. Schild, R. H. Stauber, *ACS Nano* **2011**, 5, 7155.
- [89] K. Schlich, K. Hund-Rinke, *Environ. Pollut.* **2015**, 196, 321.
- [90] European Parliament and Council of the European Union, *Off. J. Eur. Union* **2011**, 304, 18.
- [91] J. Mast, L. Demeestere, *Diagn. Pathol.* **2009**, 4, 5.
- [92] M. P. Monopoli, A. S. Pitek, I. Lynch, K. A. Dawson, in *Nanomaterial Interfaces in Biology: Methods and Protocols*, Vol. 1025 (Eds: P. Bergese, K. Hamad-Schifferli), Springer, NY **2013**, Ch. 11.
- [93] J. Pinheiro, D. Bates, S. DebRoy, D. Sarkar, R Core Team, nlme: Linear and Nonlinear Mixed Effects Models R package version 3.1-137 **2018**.
- [94] M. Kuhn, S. Weston, J. Wing, J. Forester, *The Contrast Package* **2016**.